Aquatic Mammals 2018, *44*(5), 529-537, DOI 10.1578/AM.44.5.2018.529

Relative Growth of the Skull of the Common Minke Whale (*Balaenoptera acutorostrata*) Using a 3D Laser Surface Scanner

Giacomo Franci[1] and Annalisa Berta[2]

[1]*Department of Biology, University of Pisa, Pisa, 56100, Italy*
E-mail: giacomofranci88@gmail.com
[2]*Department of Biology, San Diego State University, San Diego, CA 92182, USA*

Abstract

Growth-related morphological changes in the skulls of an ontogenetic series of 11 North Pacific common minke whales (*Balaenoptera acutorostrata*) were investigated using a three-dimensional (3D) surface laser scanner. Landmark coordinate measurements were taken at 30 points on the skull to extract individual allometric equations relating the length and zygomatic width of the skull. Comparisons were made with estimates of the surface areas of various skull components. The results revealed that the anatomical components involved in feeding (i.e., rostrum) increased in size relative to skull length. In contrast, sensory organs and the anatomical regions involved in neurological function (i.e., orbit, tympanic bullae, and foramen magnum) were fully developed at birth, and their relative size decreased over the course of development. Geometric morphometric studies such as the one described herein benefit from the capture of 3D images of specimens, making the process of sample acquisition faster, less expensive, and more readily available to researchers.

Key Words: geometric morphometrics, 2D and 3D images, allometry, minke whale, *Balaenoptera acutorostrata*

Introduction

Morphology is a key to understanding the diversity and evolutionary history of life, as well as the physical and biological interactions of species. The origin and functional consequences of variation in the shape of biological organisms has intrigued biologists for centuries (Thompson, 1917). The description and analysis of shape differences has been traditionally done using multivariate techniques based on measured distances (Blackith & Reyment, 1971). The development of geometric morphometrics (GM) (Rohlf & Marcus, 1993), which is based on the principle that spatial relationships between anatomical landmarks represent homologous biological structures, has revolutionized the study of biological shape variation (Van der Niet et al., 2010). The main advantage of GM over traditional multivariate morphometrics is that the geometric relationships among the structures are also quantified, allowing powerful interpretation and visualization of the results (Rohlf & Marcus, 1993; Adams et al., 2004). The number of studies applying this method has increased exponentially during the past few decades (Adams et al., 2004), and GM is now frequently used in specimen-based research in zoology, archaeology, and paleontology (e.g., Lawing & Polly, 2010; Sholts et al., 2011).

In the last decade, the number of studies using measurements obtained from 2D and 3D images has also increased (e.g., Loy & Slice, 2010; Sholts et al., 2011). At present, 3D digital models of specimens for morphometric analysis are relatively inexpensive and easy to acquire. These models can be successfully obtained using CT and MRI scanners for imaging internal structures or using optical surface scanners to capture digital models of the external surfaces of specimens (Sholts et al., 2011). It is also possible to obtain 3D models from 2D images in a technique known as photogrammetry. In photogrammetry, it is important to use a digital camera with high resolution, and image noise, shadows, and the reflective surfaces of the object need to be taken into account. Bone surfaces are often very reflective, which may impede visualization of important features such as skull sutures and may distort portions of the skull. The process involves taking a series of photographs of an object from different angles to generate a 3D computational model by comparing key landmark features among photographs (Mallison & Wings, 2014).

Approaches to GM data collection continue to advance rapidly. Today, 3D laser surface scanners are becoming increasingly common. In many ways,

existing coordinate-based geometric morphometric methods are not easily extendable to 3D data. This is because of difficulties in mapping coordinates onto surfaces so that they are in homologous positions (Lawing & Polly, 2010). Three-dimensional scanners create a point cloud on the surface of the subject, often by triangulation.

A number of studies have described and evaluated methods for the 3D recording of specimens housed in museum collections (Sholts et al., 2011; Mathys et al., 2013). Three-dimensional scanners share several traits with cameras, including a cone-shaped field of view, and they can only collect information about surfaces that are not obscured. While a camera collects color information, a 3D scanner also collects distance information (Bernardini & Rushmeier, 2002).

For most museum specimens, a single scan will not produce a complete model of the subject. Multiple scans from many different directions are usually required to obtain enough information about a subject. These scans must be brought into a common reference system in a process that is called alignment or registration, and then merged to create a complete model (Bernardini & Rushmeier, 2002). With the availability of 3D scanners and recent technological advances, the estimation of surface area measurements can be done using software to select the region of interest in an image and calculate its area.

The main objective of this research is to examine an ontogenetic series of North Pacific common minke whales (*Balaenoptera acutorostrata*) using geometric morphometrics and multivariate allometry of 3D images of their skulls to elucidate patterns of relative skull growth in this species. In this study, 3D laser scanning was also employed to estimate the area of the various functional components of the minke whale skull. Results were compared with those from a similar study (Nakamura & Kato, 2014) that differed in the manual acquisition of 2D measures rather than 3D skull measurements.

Methods

Data were collected from the skulls of the common minke whale using a desktop 3D laser surface scanner and the software *Scan Studio HD* (NextEngine, Santa Monica, CA, USA). The examined specimens are housed in the following institutions in California: San Diego Natural History Museum (SDNHM), Natural History Museum of Los Angeles County (LACM) in Los Angeles, Museum of Vertebrate Zoology (MVZ) in Berkeley, California Academy of Science (CAS) in San Francisco, The Marine Mammal Center (TMMC) in Sausalito, and Humboldt State University (HSU) in Arcata.

Growth was assessed by examining ontogenetic variation among skulls with a range of ages between calf, juvenile, and adult. The approximate age class of the skulls was established with reference to total body length following Walsh & Berta (2011). When the age class of the skulls could not be determined from body length, the relative age was determined based on various skull proportions of the specimens examined. Study specimens included four males: Calves HSU 2670 and LACM 72507, and Juveniles LACM 95388 and MVZ 126873; five females: Juvenile TMMC and Adults LACM 54808, HSU 7504, HSU 7503,

Figure 1. Photos of minke whale (*Balaenoptera acutorostrata*) specimens to illustrate use of the 3D laser scanner and 3D model obtained

and CAS 23867; and one specimen of unknown sex: Adult LACM 54573.

The skulls were positioned on a raised horizontal plane to facilitate examiner mobility around the specimen. The scanner was placed at an optimal focal distance (between 43 to 56 cm) from the skull, perpendicular to its horizontal plane. The scanner was gradually moved along the same plane to obtain 3D images of the dorsal portion of the skull. The ventral portion of the skull was scanned next, and images were aligned using *Scan Studio HD* software. The scanning technique and alignment process are shown in Figure 1.

A total of 30 length, width, and height measurements were obtained from each specimen (Table 1; Figure 2) following Nakamura & Kato (2014). Measurements of vomer length (VL) and minimum width of tympanic bulla (MWTB) were not obtained and were excluded from analysis.

Principal Component Analysis (PCA) was used to extract the correlation matrix and to obtain the value of the eigenvectors in the allometric analysis of the surfaces. Linear regression analysis was also performed to assess skull growth and to extract the allometric equation.

Measurements of various skull components were also collected using 3D images to determine whether they increase in surface area during development (Figure 3). Measurements were taken using the software *Geomagic Viewer* (3D system; Rock Hill, SC, USA). The surfaces obtained were then analyzed by linear regression and allometric analysis.

Results

Most of the components of the minke whale skull had a high degree of correlation with condylobasal length (CBL) (Table 2), except the nasal bones, condyles, foramen magnum, and tympanic bullae. The nasal bones and condyles had a higher correlation in width than in length with the other parts of the skull. The foramen magnum and tympanic bullae were not correlated with other components of the skull (Table 2).

Linear regression analyses suggested that many components of the skull of *B. acutorostrata* showed linear growth during development from calf to adult stage (Figure 4), with the exception of nasal bones, condyles, palatine bones, foramen magnum, ocular orbit, and tympanic bullae. The nasal bones (NL, NWA, and NW½) and condyles (OCsW, OCH, and OCW) showed a low rate of growth and grew more in width than in length. The palatine bones (PaL and PAWP) showed more prominent growth in length and less in width. The foramen magnum (FMW and FMH) increased slightly in width from calf to adult

Table 1. Skull measurements and abbreviations used in this study

	Measurement	Abbreviation		Measurement	Abbreviation
1	Condylobasal length	CBL	16	Foramen magnum width	FMW
2	Maxilla length	MaL	17	Foramen magnum height	FMH
3	Premaxilla length	PmL	18	Width of occipital condyles	OCsW
4	Rostrum length	RL	19	Occipital condyles height	OCH
5	Rostrum width at the middle	RW ½	20	Occipital condyles width	OCW
6	Rostrum width at the antorbital notch	RW	21	Tip of premaxilla to the posterior edge of the squamosal	TPm-PS
7	Skull width at the outer edge of posterior edge of maxilla	SWPMa	22	Tip of premaxilla to the posterior edge of the occipital bone	TPm-POB
8	Skull width at postorbital process of the frontal bone	SWPPF	24	Palatine length	PaL
9	Zygomatic width of the skull	ZW	25	Palatine width at posterior end	PaWP
10	Greatest width of the occipital bone	GWOB	26	Tympanic bulla length	TBL
11	Length from the upper ridge of foramen magnum to superior part of the occipital bone	UFM-SPOB	27	Greatest width of tympanic bulla	GWTB
12	Nasal length	NL	29	Tympanic bulla height	TBH
13	Nasal width at the anterior edge of the process	NWA	30	Skull height	SH
14	Nasal width at the midpoint	NW½	31	Orbit height	OH
15	Minimum width of the parietal bone	MWP	32	Orbit width	OW

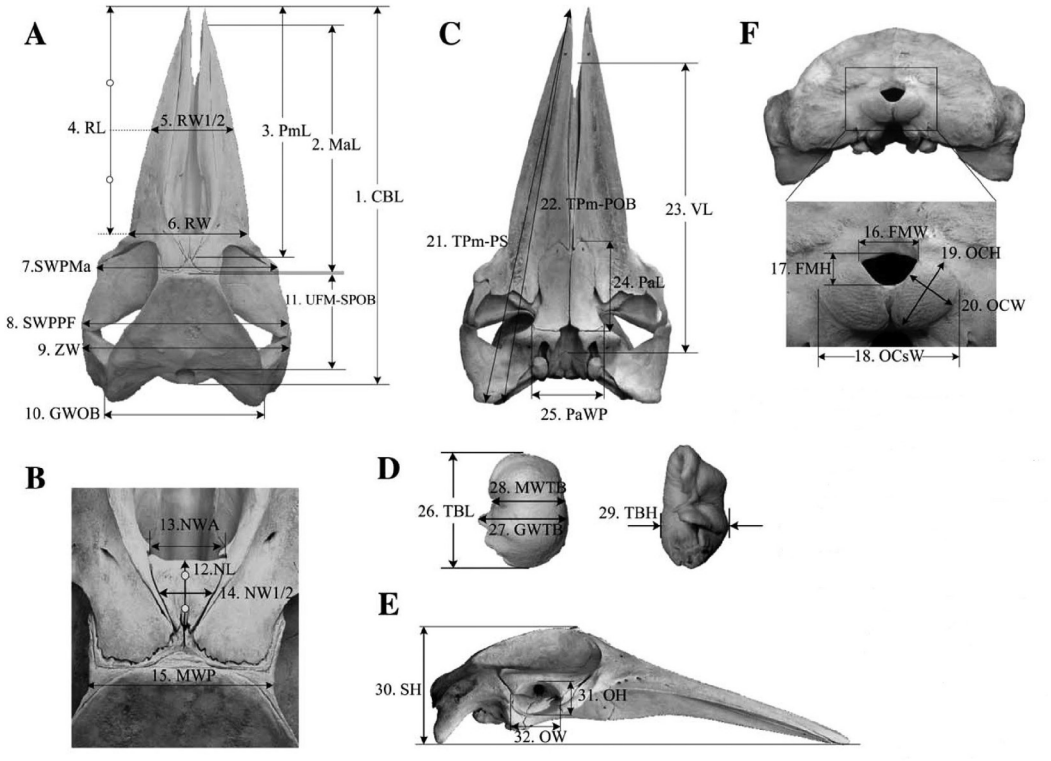

Figure 2. Skull measurements taken on *B. acutorostrata* (modified from Nakamura & Kato, 2014): (A) dorsal view, (B) nasal bones, (C) ventral view, (D) tympanic bulla, (E) lateral view, and (F) posterior view.

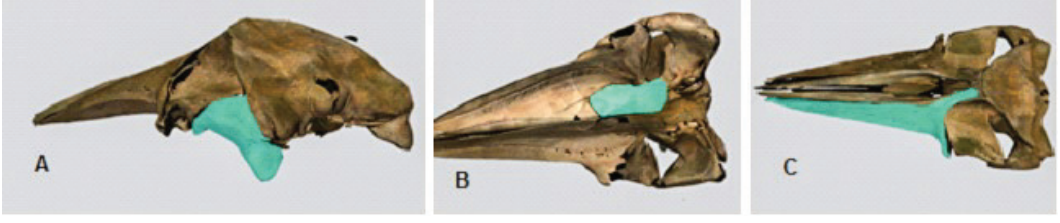

Figure 3. Examples of skull surface area selections: (A) squamosal, zygomatic, and postglenoid complex; (B) palatine; and (C) maxilla.

while remaining relatively unchanged in height. A decrease in proportion with condylobasal length (CBL) was observed. Orbit height (OH) showed no signs of growth; rather, it had a similar size in the three individuals where it was possible to measure this dimension. The tympanic bullae (TBL, GWTB, and MWTB) did not increase in size from the juvenile to adult stage.

Allometric analysis (Table 3) indicated the condylobasal length (CBL) of the skull exhibited isometric allometry. This is in contrast to the allometry observed in the length of the rostrum (RL) that was positive and the length of the occipital plate (UFM-SPOB) that was negative. The height of the skull (SH) also exhibited negative allometry. The length measurements of the ventral part of the skull (TPm-PS and TPm-POB) showed isometric growth with condylobasal length. The width of the skull showed negative allometry for the measurements made on ZW and GWOB. SWMPa and SWPPF, instead, had isometric coefficients. All the components of the rostrum showed the highest allometric coefficients observed regarding length measurements (MaL, PmL, and RL). Mid rostrum width (RW½) also had positive allometry, while the rostrum width at the antorbital notch (RW) had negative allometry. The palatines showed isometry in

Table 2. Correlation coefficients (r) of measurement taken related to condylobasal length (CBL): r = correlation coefficient, $r > 0$ positive correlation, $r < 0$ negative correlation, and $r = 1$ linear correlation.

Correlation coefficients of measurements relative to condylobasal length (CBL)	
Measurement site	*r*
2. Maxilla length (MaL)	0.993
4. Rostrum length (RL)	0.996
9. Zygomatic width (ZW)	0.983
10. Greatest width of the occipital bone (GWOB)	0.980
12. Nasal length (NL)	0.736
13. Nasal width at the anterior edge of the process (NWA)	0.900
15. Minimum width of the parietal bone (MWP)	0.900
16. Foramen magnum width (FMW)	-0.334
17. Foramen magnum height (FMH)	0.394
18. Width of occipital condyles (OcSW)	0.938
19. Occipital condyles height (OCH)	0.795
20. Occipital condyles width (OCW)	0.932
26. Tympanic bulla length (TBL)	-0.376
27. Greatest width of tympanic bulla (GWTB)	-0.361
30. Skull height (SH)	0.983

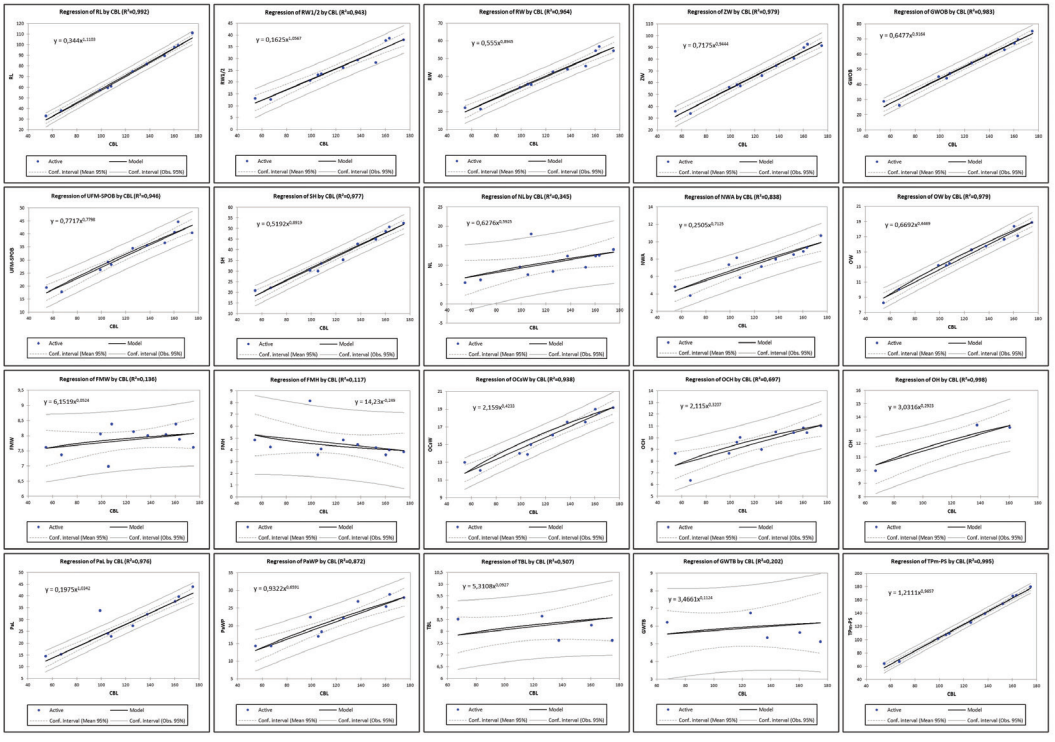

Figure 4. Linear regressions of various skull measurements of minke whales

Table 3. Relative growth coefficients and relative growth patterns of each part of the skull of minke whales: α = relative growth coefficient and lnβ = growth constant. The relative growth pattern was classified as "Positive" when the relative growth coefficient was significantly larger than 1, "Negative" when the coefficient was significantly smaller than 1, and "Isometric" when the coefficient did not differ significantly from 1.

Measurement	α	lnβ	Relative growth pattern
1. Condylobasal length (CBL)	1.03	1.62	Isometric
2. Maxilla length (MaL)	1.06	0.53	Positive
3. Premaxilla length (PmL)	1.07	0.50	Positive
4. Rostrum length (RL)	1.11	0.34	Positive
5. Rostrum width at the middle (RW½)	1.06	0.16	Positive
6. Rostrum width at the antorbital notch (RW)	0.9	0.56	Negative
7. Skull width at the outer edge of posterior edge of maxilla (SWPMa)	0.97	0.55	Isometric
8. Skull width at postorbital process of the frontal bone (SWPPF)	0.96	0.62	Isometric
9. Zygomatic width of the skull (ZW)	0.94	0.71	Negative
10. Greatest width of the occipital bone (GWOB)	0.92	0.65	Negative
11. Length from the upper ridge of foramen magnum to superior part of the occipital bone (UFM-SPOB)	0.78	0.77	Negative
12. Nasal length (NL)	0.59	0.63	Negative
13. Nasal width at the anterior edge of the process (NWA)	0.71	0.25	Negative
14. Nasal width at the midpoint (NW½)	0.87	0.08	Negative
15. Minimum width of the parietal bone (MWP)	0.73	0.49	Negative
16. Foramen magnum width (FMW)	0.05	6.15	Negative
17. Foramen magnum height (FMH)	-0.25	14.23	Negative
18. Width of occipital condyles (OCsW)	0.42	2.16	Negative
19. Occipital condyles height (OCH)	0.32	2.12	Negative
20. Occipital condyles width (OCW)	0.70	0.22	Negative
21. Tip of premaxilla to the posterior edge of the squamosal (TPm-PS)	0.97	1.21	Isometric
22. Tip of premaxilla to the posterior edge of the occipital bone (TPm-POB)	0.97	1.20	Isometric
24. Palatine length (PaL)	1.03	0.20	Isometric
25. Palatine width at posterior end (PaWP)	0.66	0.93	Negative
26. Tympanic bulla length (TBL)	0.09	5.31	Negative
27. Greatest width of tympanic bulla (GWTB)	0.11	3.47	Negative
29. Tympanic bulla height (TBH)	0.06	3.44	Negative
30. Skull height (SH)	0.89	0.52	Negative
31. Orbit height (OH)	0.29	3.03	Negative
32. Orbit width (OW)	0.65	0.67	Negative

length and negative allometry in width. Negative allometry was observed for nasal bones (NL, NWA, and NW½), condyles (OCsW, OCH, and OCW), foramen magnum (FMW and FMH), tympanic bullae (TBL, GWTB, and MWTB), and the orbit (OH and OW). The foramen magnum, tympanic bullae, and orbit height showed the lowest allometric coefficients (Table 3).

From the analysis of surfaces (Table 4), the rostrum showed the highest allometric coefficient. Despite the negative allometry of the braincase, many of its components (occipital, palatines, parietal, and frontals) showed positive allometry. The frontal bones had the highest allometric coefficient between all components of the braincase. The condyles had a negative allometric coefficient, showing that growth of this surface area is minimal. The squamosal, zygomatic, and postglenoid complex (ZSP) also had a negative allometric coefficient.

Table 4. Relative growth patterns of each part of the skull of minke whales based on eigenvectors, where *p* is the number of measurements. The difference is the allometric coefficient: greater than 0 indicates positive allometry, 0 value indicates isometric growth, and less than 0 indicates negative allometry.

Measurement site	Eigenvectors	(1/*p*)^1/2	Difference	Relative growth pattern
Maxilla top	0.309	0.289	0.02	Positive
Maxilla ventral	0.314	0.289	0.025	Positive
Maxilla total	0.313	0.289	0.024	Positive
Occipital	0.302	0.289	0.013	Positive
Palatine	0.304	0.289	0.015	Positive
Frontal	0.308	0.289	0.019	Positive
Condyl	0.124	0.289	-0.165	Negative
Parietal	0.301	0.289	0.012	Positive
ZSP	0.219	0.289	-0.07	Negative
Rostrum	0.314	0.289	0.025	Positive
Braincase	0.279	0.289	-0.01	Negative
Total surface	0.313	0.289	0.024	Positive

Discussion

Previous studies on the morphology of mysticetes were primarily based on manual measurements (obtained using a tape or caliper) of various skeletal and skull components or on measurements taken from photos or models obtained through the capture of 2D images. The precision and repeatability of measurements collected in different studies using varied instruments is still an issue that deserves further attention (Sholts et al., 2013). Using landmark analysis of 2D images of the dorsal surface of the skull, Hampe & Baszio (2010) showed evidence of evolutionary changes in the skull shape of extinct mysticetes (i.e., Aetiocetidae) and extant balaenopterid mysticetes (e.g., *B. acutorostrata, Balaenoptera physalus*, and *Megaptera novaeangliae*).

In the current study, many components of the minke whale skull that exhibited growth in size were correlated, except for the nasal bones, condyles, foramen magnum, and tympanic bullae. These are similar to some of the results obtained by Nakamura & Kato (2014). In the latter study, the rostrum showed growth during development. The orbit, nasal bones, tympanic bullae, foramen magnum, occipital condyles, and other regions that surround neural components showed less growth during development. In the present study, the growth of the tympanic bullae, foramen magnum, and orbit were near completion at birth.

Some of our results, however, differ from those of Nakamura & Kato (2014). We observed isometry of the condylobasal length (CBL) and negative allometry of the occipital length (UFM-SPOB) and height of the skull (SH). Nakamura & Kato, instead, observed negative allometry of CBL and positive allometry of UFM-SPOB and SH. We noted negative allometry or isometry for all the observations in width of the cranium (SWPMa, SWPPF, ZW, and GWOB) and width of the rostrum (RW), which were reported as positive by Nakamura & Kato. The ventral length from the tip of the premaxilla to the posterior edge of the squamosal and to the occipital (TPm-PS and TPm-POB), and the palatine length (PaL) were isometric with condylobasal length rather than positive. The length and width of the nasal (NL and NWA) were negatively allometric in our study rather than positively allometric and isometric as observed by Nakamura & Kato.

The positive allometry of the components of the rostrum indicates that the growth of the skull in *B. acutorostrata* is more prominent for the feeding apparatus during development. All balaenopterids feed through engulfment of prey, a process that is energetically expensive (Lambertsen et al., 1995). The size of the skull and jaws play a fundamental role in this process. Most *Balaenoptera* species have a proportionally large head relative to body size when compared to other mammals (Goldbogen, 2010). Minke whales, however, are smaller in overall body length than other species of *Balaenoptera* and have a relatively small head. This small head may help to reduce drag and enhance locomotor performance when feeding.

Since minke whales prey on small fish (Folkow et al., 2000), a small head may be an advantage for capturing small and therefore relatively more agile prey. This may explain why the length and width of the skull are isometric, despite the positive allometry in the length of the rostrum that creates a tapered head shape.

The overall differences in skull growth observed in this study and in Nakamura & Kato (2014) could be attributed to various factors such as differences in specimen availability and methods used. This study employed 3D imaging instead of manual measurements or 2D images as has been more common in past studies. Future comparisons of different methods (e.g., 2D vs 3D) may be useful for evaluating the effectiveness of both. Due to the lack of male and female specimens of the same age class, the influence of sexual dimorphism on skull growth was not measured in this study.

A major advantage of using 3D images is the possibility of calculating surface areas of specific parts of the specimens. Geometric morphometric analyses of shape based solely on linear measurements often do not capture the overall growth of the specimen. Volume and growth cannot be accurately measured using linear measurements alone. For example, in addition to showing that the surface of the occipital exhibited positive allometry, our measurements of surface areas in various portions of the minke whale confirmed the increased growth rate of the rostrum compared to the braincase. This may be due to some bones acquiring a concave or convex shape during development instead of linearly increasing in length or width. Previous studies have suggested that the use of 3D laser surface scanners and the reconstruction of 3D models is time consuming for large whale skulls (Mathys et al., 2013). Some of the issues found when capturing images within concave structures (e.g., linear distortions) could be solved by using a CT scanner. Since the specimen does not need to be reoriented multiple times during CT scanning, the process of data acquisition is faster. However, as most large whale skulls are too big for a CT scanner, they are ideal candidates for 3D laser surface technology.

The sampling and processing of data from 3D images provide many research possibilities. Until recently, linear measurements were often the norm when describing specimens, but 3D images and specialized software allow the generation of surface and volumetric measurements.

Several geometric morphometric databases for primate and human fossils are available (e.g., PRIMO and USNM). Future research efforts should allow for the collection and public availability of digital images of specimens in museum collections. Access to databases of digital images of specimens would enhance their study, particularly for large specimens. It would also reduce costs of research (allowing access without travel) and potentially minimize damage to the collections (due to excessive specimen handling). For this, image data banks should meet some basic requirements, including standards for image recording, acquisition, storage, and analysis of morphometric information. Future scientific research would be potentially enhanced with the basic capacity to search and download images (2D or 3D) of museum specimens that are otherwise difficult to access and handle (Loy & Slice, 2010).

Acknowledgments

We wish to express gratitude to Giovanni Bianucci (University of Pisa), Thomas Deméré (SDNHM), Eric Ekdale (SDSU), Kesler Randall (SDNHM), David Janiger (LACM), Sue Pemberton (CAS), Chris J. Conroy (MVZ), and Thorvald Holmes, Jr. (HSU) for access to specimens and discussion, and to the University of Pisa for providing financial support to GF.

Literature Cited

Adams, D. C., Rohlf, F. J., & Slice, D. E. (2004). Geometric morphometrics: Ten years of progress following the "revolution." *Italian Journal of Zoology*, *71*(1), 5-16. https://doi.org/10.1080/11250000409356545

Bernardini, F., & Rushmeier, H. (2002). The 3D model acquisition pipeline. *Computer Graphics Forum*, *21*(2). https://doi.org/10.1111/1467-8659.00574

Blackith, R. E., & Reyment, R. A. (1971). *Multivariate morphometrics*. London: Academic Press.

Folkow, L. P., Haug, T., Nilssen, K. T., & Nordøy, E. S. (2000). Estimated food consumption of minke whales *Balaenoptera acutorostrata* in northeast Atlantic waters in 1992-1995. *NAMMCO Science Publications*, *2*, 65-80. https://doi.org/10.7557/3.2972

Goldbogen, J. A. (2010). The biomechanics of whale feeding. *American Scientist*, *98*, 124-131. https://doi.org/10.1511/2010.83.124

Hampe, O., & Baszio, S. (2010). Relative warps meet cladistics: A contribution to the phylogenetic relationships of baleen whales based on landmark analyses of mysticete crania. *Bulletin of Geosciences*, *85*(2), 199-218. https://doi.org/10.3140/bull.geosci.1166

Lambertsen, R., Ulrich, N., & Straley, J. (1995). Frontomandibular stay of Balaenopteridae: A mechanism for momentum recapture during feeding. *Journal of Mammalogy*, *76*(3), 877-899. https://doi.org/10.2307/1382758

Lawing, A. M., & Polly, P. D. (2010). Geometric morphometrics: Recent applications to the study of evolution and development. *Journal of Zoology*, *280*(1), 1-7. https://doi.org/10.1111/j.1469-7998.2009.00620.x

Loy, A., & Slice, D. E. (2010). Image data banks and geometric morphometrics. In P. L. Nimis & R. V. Lebbe (Eds.), *Tools for identifying biodiversity: Progress and problems* (pp. 243-248). Trieste, Italy: EUT Edizioni Università di Trieste.

Mallison, H., & Wings, O. (2014). Photogrammetry in paleontology: A practical guide. *Journal of Paleontological Techniques*, *12*, 1-31.

Mathys, A., Brecko, J., & Semal, P. (2013). Comparing 3D digitizing technologies: What are the differences? In *Digital Heritage International Congress* (Vol. 1, pp. 201-204). Piscataway, NJ: Institute of Electrical and Electronics Engineers (IEEE). https://doi.org/10.1109/DigitalHeritage.2013.6743733

Nakamura, G., & Kato, H. (2014). Developmental changes in the skull morphology of common minke whales *Balaenoptera acutorostrata*. *Journal of Morphology*, *275*, 1113-1121. https://doi.org/10.1002/jmor.20288

Rohlf, F. J., & Marcus, L. F. (1993). A revolution in morphometrics. *Trends in Ecology & Evolution*, *8*(4), 129-132. https://doi.org/10.1016/0169-5347(93)90024-J

Sholts, S. B., Flores, L., Walker, P. L., & Warmlander, S. K. T. S. (2011). Precision of different landmark types on human crania using 3D laser scanner and a 3D digitiser: Implications for applications of digital morphometrics. *International Journal of Osteoarchaeology*, *21*, 535-543. https://doi.org/10.1002/oa.1156

Thompson, D. W. (1917). *On growth and form*. Cambridge, UK: Cambridge University Press. 793 pp. https://doi.org/10.5962/bhl.title.11332

Van der Niet, T., Zollikofer, C. P. E., de León, M. S. P., Johnson, S. D., & Linder, H. P. (2010). Three-dimensional geometric morphometrics for studying floral shape variation. *Trends in Plant Science*, *15*(8), 423-426. https://doi.org/10.1016/j.tplants.2010.05.005

Walsh, B. M., & Berta, A. (2011). Occipital ossification of balaenopteroid mysticetes. *Anatomical Record*, *294*, 391-398. https://doi.org/10.1002/ar.21340